Journal Pre-proof

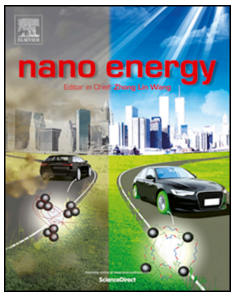

Influences of surface charges and gap width between *p*-type and *n*-type semiconductors on charge pumping

Shuo Deng, Ran Xu, Min Li, Lijie Li, Zhong Lin Wang, Qing Zhang

PII: S2211-2855(20)30864-8

DOI: https://doi.org/10.1016/j.nanoen.2020.105287

Reference: NANOEN 105287

To appear in: *Nano Energy*

Received Date: 6 July 2020

Revised Date: 30 July 2020

Accepted Date: 8 August 2020

Please cite this article as: S. Deng, R. Xu, M. Li, L. Li, Z.L. Wang, Q. Zhang, Influences of surface charges and gap width between *p*-type and *n*-type semiconductors on charge pumping, *Nano Energy* (2020), doi: https://doi.org/10.1016/j.nanoen.2020.105287.

Credit Author Statement:

Shuo Deng and Qing Zhang designed the system and wrote the paper. Shuo Deng and Lijie Li performed the calculation and analyzed the data. Ran Xu, Min Li, Zhong Lin Wang and Qing Zhang analyzed the data. Min Li, Lijie Li, Zhong Lin Wang and Qing Zhang supervised the paper.

Influences of surface charges and gap width between *p*-type and *n*-type semiconductors on charge pumping

Shuo Deng [a], Ran Xu [b], Min Li [a], Lijie Li [c], Zhong Lin Wang [d e] and Qing Zhang [b *]

[a] *Department of Physics, Wuhan University of Technology, Wuhan 430070, China*

[b] *School of Electrical & Electronic Engineering, Nanyang Technological University, Singapore 639798, Singapore*

[c] *College of Engineering, Swansea University, Swansea SA1 8EN, UK*

[d] *Beijing Institute of Nanoenergy and Nanosystems, Chinese Academy of Science, Beijing 100083, China*

[e] *School of Materials Science and Engineering, Georgia Institute of Technology, Atlanta, GA 30332, USA*

[*]Corresponding author

E-mail: eqzhang@ntu.edu.sg

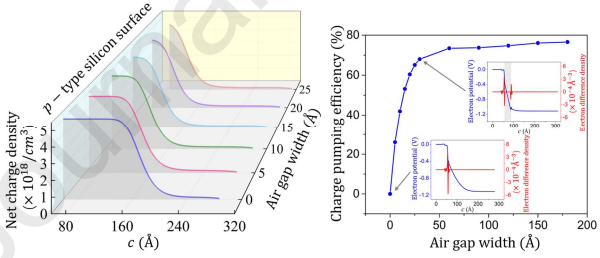

Influences of surface charges and gap width between *p*-type and *n*-type semiconductors on charge pumping

Shuo Deng [a], Ran Xu [b], Min Li [a], Lijie Li [c], Zhong Lin Wang [d e] and Qing Zhang [b *]

[a] *Department of Physics, Wuhan University of Technology, Wuhan 430070, China*
[b] *School of Electrical & Electronic Engineering, Nanyang Technological University, Singapore 639798, Singapore*
[c] *College of Engineering, Swansea University, Swansea SA1 8EN, UK*
[d] *Beijing Institute of Nanoenergy and Nanosystems, Chinese Academy of Science, Beijing 100083, China*
[e] *School of Materials Science and Engineering, Georgia Institute of Technology, Atlanta, GA 30332, USA*

[*]Corresponding author
E-mail: eqzhang@ntu.edu.sg

Abstract: It has been reported that charges can be pumped out of an intermittently contacted *p*-*n* (or Schottky) junction, accompanied with mechanical to electric power conversion [1]. The amount of charge measured in the circuit, however, was observed to be 3 ~ 4 orders of magnitudes smaller than the space charge in the depletion regions of an ideal *p*-*n* (or Schottky) junction formed with the corresponding semiconductors (or metals). In this work, charge pumping between *p*-type and *n*-type silicon is investigated using the first principles calculation with non-equilibrium Green function. We find that a large density of states is formed during silicon surface relaxation and they are further changed during hydrogenated process. The surface charges result in a surface potential barrier, which has a negative impact on electron and hole transfer between the contacted silicon surfaces. In addition, it is also found that the total charges in the depletion regions depend very sensitively on the air gap between the two silicon electrodes. More than 68% of the charges can be pumped out with a gap of 30 Å. These results suggest that intermittently contacted *p*-*n* junction could function as an efficient electric generator or mechanical sensor if the surface states and gap width are well controlled.

Key words: Electric generator, Electron pump, Non-ideal contact, *p*-*n* junction, Mechanical sensor, First principles calculation

Introduction:

Although mechanical-to-electric power conversion has been realized with several fundamental working principles, there still exists a very big challenge to miniaturize electric generators for smart applications [2-6]. Till today, many micro/nano generators have been studied to pursue an extraordinary capability of mechanical-electric power conversion [7-11]. The most extensively studied micro/nano generators are electrostatic generators [7, 8, 12-14], piezoelectric generators [9, 15, 16] and triboelectric generators [17-19]. A common characteristic of typical electrostatic, piezoelectric and triboelectric generators is that there is only displacement current, rather than conduction current, across the two electrodes so that the internal and external are coupled capacitively, leading to a very high internal resistance. In 2018, we reported an electric generator based on a pair of semiconductor electrodes with distinct chemical potentials [1]. When the two electrodes are brought in contact, electrons diffuse from the *n*-type semiconductor (higher chemical potential) to the *p*-type semiconductor (lower chemical potential) due to the chemical potential difference. Once both electrodes are separated by mechanical power, the diffused electrons can be pumped out to the external circuit. Different from typical electrostatic, piezoelectric and triboelectric nanogenerators, this generator generates both conduction current and displacement current. However, it was found that, with a prototype, actual charge output was only about 3 ~ 4 orders of magnitude smaller than the total charges in the depletion region of the ideal *p*-*n* junction formed with the corresponding doped semiconductors. The influences of non-ideal surfaces, i.e, the surface states/charges and atomic scale asperities induced non-prefect contact, on electron transfer and pumping in the intermittently contacted *p*-*n* junction still require an in-depth study.

In this work, the influences of the surface charges and gap width on electron transfer between two silicon electrodes are systematically studied using the first-principles methods with non-equilibrium Green function (NEGF) [20]. Although several theoretical studies have been reported on the influences of interface barrier and surface chemical modification on the performance of triboelectric nanogenerators [21-24], they all discussed the contact electrification between metals and polymers. To our best knowledge, no research on electron transfer between two semiconducting electrodes has been conducted using first principles calculation. Moreover, the contact electrification mechanism between two semiconducting electrodes is not clear yet [1, 25-27]. Our results demonstrate that the surface charges and small air gaps between the two contacted surfaces are the two killer factors that have significant impacts on the pumped charges to the circuit.

Computation procedure:

The first-principles calculations are performed here using Atomistic ToolKit (ATK 2019) software package [28], which is capable of investigating semiconductor devices

and surface states [29, 30]. The exchange correlation function for generalized gradient approximation (GGA) with the Perdew-Burke-Ernzerhof (PBE) in the surface relaxation calculations is utilized [31]. The *k*-points are $9 \times 9 \times 1$ and the cutoff energy is $30\ Hartree$. We begin with an ideal silicon (100) surface, whose side view is shown in Fig. 1a. The ideal silicon (100) surface is obtained by cleaving silicon (alpha) structure along (100) direction without any surface relaxation. To model a practical silicon (100) surface, we firstly relax the surface structure until the force on all atoms smaller than $0.01\ eV\text{Å}^{-1}$ with the stress error tolerance for $0.001\ eV\text{Å}^{-3}$ [32]. The side view of the relaxed silicon (100) surface is illustrated in Fig. 1b, in consistence with prior relaxed silicon (100) surface structure [32]. It is clearly seen that a few atomic layers from the surface are largely relaxed in comparison with the ideal surface (Fig.1a) as the surface relaxation is a long-range effect and it could affect a few layers beneath the surface layer. As the GGA-PBE method is not able to produce a proper bandgap in a semiconductor, we employ the meta-GGA function for the electronic structure calculations [33, 34]. In our electron transfer calculation, the brillouin zone of the silicon *p-n* junction is sampled by a $7 \times 7 \times 100$ *k*-mesh with a double-zeta polarized basis for all atoms. In the electron transfer regime, the *I-V* curves are calculated using the NEGF [20]. The current across the silicon *p-n* junction can be calculated as follows:

$$I = \frac{e}{h}\int_{\mu_L}^{\mu_R} \left(f_L(E) - f_R(E) \right) T_e(E)\, dE\,, \qquad (1)$$

where, $f_L(E)$ ($f_R(E)$) and μ_L (μ_R) are the Fermi distribution function and chemical potential of the left (right) electrode, which are directly correlated with their doping concentrations. T_e is the electron transmission function and reflects the impact of the surface charges and gap width on electron transfer. e and h are the unit charge and Planck's constant, respectively. The spectral density matrix, $\rho(E)$, can be calculated from the density matrix contributions from the left and right electrodes:

$$\rho(E) = \rho^L(E) + \rho^R(E)\,. \qquad (2)$$

The local density of states, $D(E,r)$, is calculated from the spectral density matrix:

$$D(E,r) = \sum_{ij} \rho_{ij}(E)\phi_i(r)\phi_j(r)\,, \qquad (3)$$

where $\phi(r)$ is the real functions in solid harmonics, i and j are the electron orbitals. Then, the device density of states, $D(E)$, of the relaxed silicon surfaces is calculated by integrating the local density of states over the space:

$$D(E) = \int D(E,r)\, dr\,. \qquad (4)$$

The electron difference density (EDD) in the *p-n* junction, $\Delta n(r)$, is defined as:

$$\Delta n(r) = n(r) - \sum_{I}^{N_{atoms}} n_I(r)\,, \qquad (5)$$

where $n(r)$ is the electron density, $n_I(r)$ is the electron density of atom I and N_{atoms} is the number of atoms in the *p-n* junction. The relation between Hartree

difference potential (HDP), $\Delta V_H(r)$, and EDD can be determined using the Possion equation:

$$\nabla^2 \Delta V_H(r) = -\frac{e^2}{4\pi\varepsilon_0}\Delta n(r), \qquad (6)$$

where ε_0 is the vacuum permittivity. From Eq. (2) to Eq. (6), the energy band diagram along the electron transfer direction for the contacted *p-n* junction can be obtained.

Results and Discussion:

Figs. 1c and 1d show the DOS of silicon (100) surface without and with the surface relaxation, respectively. From Fig. 1c, one can see that the DOS of surface layer (1, 2) of the ideal surface is very similar to that of the internal layer (6, 7) around the conduction band minimum (CBM) and the valence band maximum (VBM), suggesting that the interaction between the silicon surface and internal is negligible. In the surface relaxation, silicon (100) surface first forms a symmetric dimer which in turns induces an asymmetry in the electron landscape, under which we again optimize the structure to find the ground state asymmetric structure. After the surface relaxation, the relaxed silicon surface is in reasonable consistence with a previous study where an asymmetric dimer reconstruction of silicon (100) surface was built [27]. The bandgap is reduced by around $0.31\,eV$ (Fig. 1d) and a peak at the VBM is formed predominantly for the surface layers (1, 2), indicating a large influence of the relaxed silicon surface on the electronic states. Besides, the DOS of the internal layer (6, 7) shows only small difference from the ideal silicon surface in the whole energy range because the surface relaxation progress could affect a few layers beneath the surface layer. Obviously, the surface relaxation plays a prominent role not only in reaching the minimum free energy to have a higher stability, but also in the distribution of the surface electronic states.

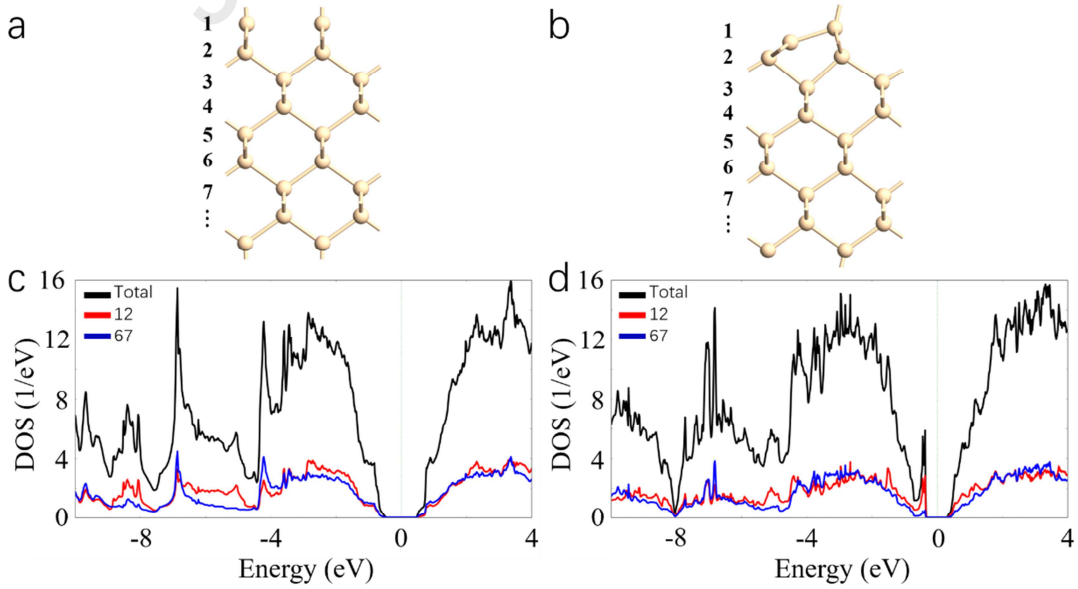

Fig. 1. The side view and DOS of the ideal and relaxed silicon (100) surface. a and

b, The side-view of the ideal and relaxed silicon (100) surface, respectively. Layers 1 and 2 for the relaxed silicon surface in **b** are largely relaxed in comparison with layers 1 and 2 for the ideal silicon surface in **a**. **c** and **d,** The DOS of the ideal and relaxed silicon (100) surface, respectively. After the surface relaxation, the bandgap is reduced and a peak at the VBM is formed in **d**, indicating a large influence of the surface relaxation on the electronic states.

The ideal silicon *p*-*n* junction is formed through a perfect contact of an ideal *n*-type silicon (100) surface with another ideal *p*-type silicon (100) surface (Fig 1a), without leaving any dangling bonds or defects at the contacted interface. Thus, the ideal *p*-*n* junction can be regarded as a *p*-*n* junction formed by donor or acceptor diffusion/implantation processes in bulk silicon. In sharp contrast, the non-ideal *p*-*n* junction is constructed by a relaxed *n*-type silicon surface intimately contacted with a relaxed *p*-type silicon surface (Fig. 1b). All the surface dangling bonds are terminated by hydrogen atoms. Hydrogenation treatment here is in line with our previous experiments where silicon electrodes were treated in HF to have a higher mechanical to electric power conversion efficiency [1]. The accepter concentration for the *p*-type silicon and donor concentration for the *n*-type silicon are selected to be 1×10^{20} and $5 \times 10^{18}\ cm^{-3}$, respectively, for the following discussion. Fig. 2a shows the *I*-*V* curves of the ideal and non-ideal silicon *p*-*n* junctions. Although both *p*-*n* junctions exhibit apparent rectification characteristics, the current density of the ideal *p*-*n* junction is 1 ~ 2 order(s) of magnitude higher than that of the non-ideal *p*-*n* junction for the bias voltage between 0 and $1.0\,V$. This suggests the non-ideal contact hinders electron transfer across the contacted relaxed surfaces. In the ideal *p*-*n* junction, the HDP decreases monotonically from the *p*-type to the *n*-type silicon across the entire *p*-*n* junction (Fig. 2b). The depletion region width in the *n*-type silicon, W_n (from the *n*-type silicon surface to the edge where $\Delta n(r) = 0$) is about 195 Å. In contrast, the relaxed non-ideal surface introduces a perturbance in the HDP at the contacted surfaces so that HDP decays much faster than the ideal *p*-*n* junction and the depletion region width W_n' is only 170 Å (Fig. 2b). Figs. 2c and 2d show the energy band diagrams of the ideal and non-ideal silicon *p*-*n* junction, respectively. With the accepter concentration being 2 orders of magnitude higher than the donor concentration, the depletion region width in the *p*-type silicon is much smaller than that in the *n*-type silicon. Note that the donor concentration of the *n*-type silicon electrode in this work is about 3 orders of magnitude higher than that used in the previous experiments [1]. Selection of a higher donor concentration here is restrained by our calculation capability. Nevertheless, evaluation of the influences of the surface charges on electron transfer is not affected by selection of the donor or acceptor concentrations. The energy band diagrams across the entire ideal and non-ideal *p*-*n* junctions are shown in Figs. 2c and 2d. A band gap of $1.16\ eV$ can be extracted at the two back ends of the silicon electrodes. Being consistent with the HDP distribution, an apparent “abyss” in the energy band diagram occurs in the non-ideal contacted *p*-*n* junction.

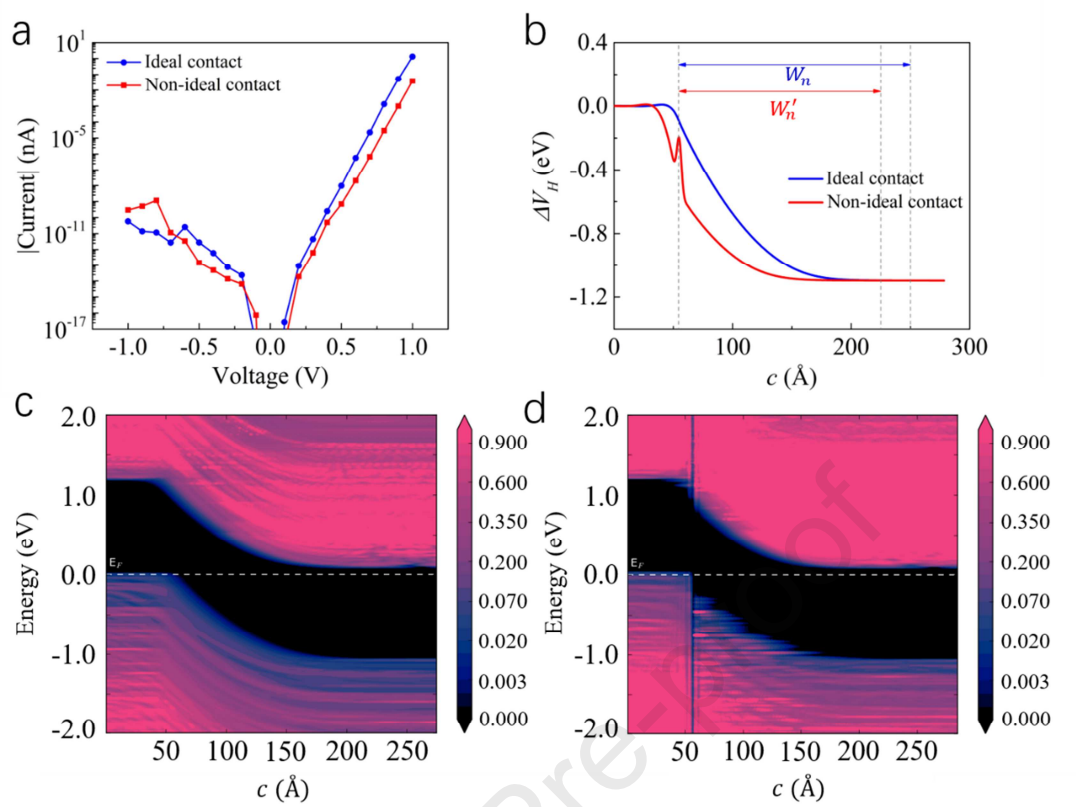

Fig. 2. Electron transport property of the ideal and non-ideal contact *p-n* junction. a, The *I-V* curves and **b**, the HDP results for the ideal and non-ideal *p-n* junction. The current density and depletion region width of the ideal *p-n* junction are significantly larger than those of the non-ideal *p-n* junction, respectively, suggesting the non-ideal contact hinders electron transfer across the contacted relaxed surfaces. **c** and **d**, The energy band diagrams for the ideal and non-ideal *p-n* junction, respectively. An apparent "abyss" in the energy band diagram occurs in the non-ideal contacted *p-n* junction.

To study the influence of the doping concentrations on the HDP distribution in the non-ideal contacted *p-n* junction, several different donor and acceptor concentrations are selected. First, the calculation is conducted by increasing the accepter concentration, N_A, from 5×10^{19} to $5 \times 10^{20}\ cm^{-3}$, while keeping the donor concentration, N_D, unchanged at $5 \times 10^{18}\ cm^{-3}$ (Fig. 3a). The calculation is then repeated with N_D increasing from 1×10^{18} to $1 \times 10^{19}\ cm^{-3}$, while keeping N_A unchanged at $1 \times 10^{20}\ cm^{-3}$ (Fig. 3b). A general trend is that the depletion width increases with decreasing the doping concentration and the perturbance in the HDP distribution at the non-ideal contacted surfaces is more sensitively dependent on N_D than N_A. It is also seen that the HDP distribution is not perfectly converged with the device length of ~ 300Å for $N_D \sim 1 \times 10^{18}\ cm^{-3}$, see the black curve in Fig. 3b. With $N_A \sim 1 \times 10^{20}\ cm^{-3}$ and $N_D \sim 5 \times 10^{18}\ cm^{-3}$ (used in Fig. 2b), the HDP distribution is found to be fully converged within the device length, see the red curve in Fig. 3b. The EDD at the relaxed surfaces is noticeably modulated by N_D rather than N_A, as shown in Figs. 3c and 3d. The positive and negative values of the EDD

depict electron aggregation and depletion, respectively. Hydrogen atoms (the surface passivation layer) tend to gain electrons from the bulk silicon as hydrogen atoms are more electronegative than silicon atoms, forming a negative surface charge layer. Clearly, the perturbance in the HDP is induced by the EDD at the surfaces, or, in other words, the surface charges. The details of the EDD at the edge of the depletion regions in the *n*-type silicon can be seen by the zoom-in views in the inset in Figs. 3c and 3d, respectively.

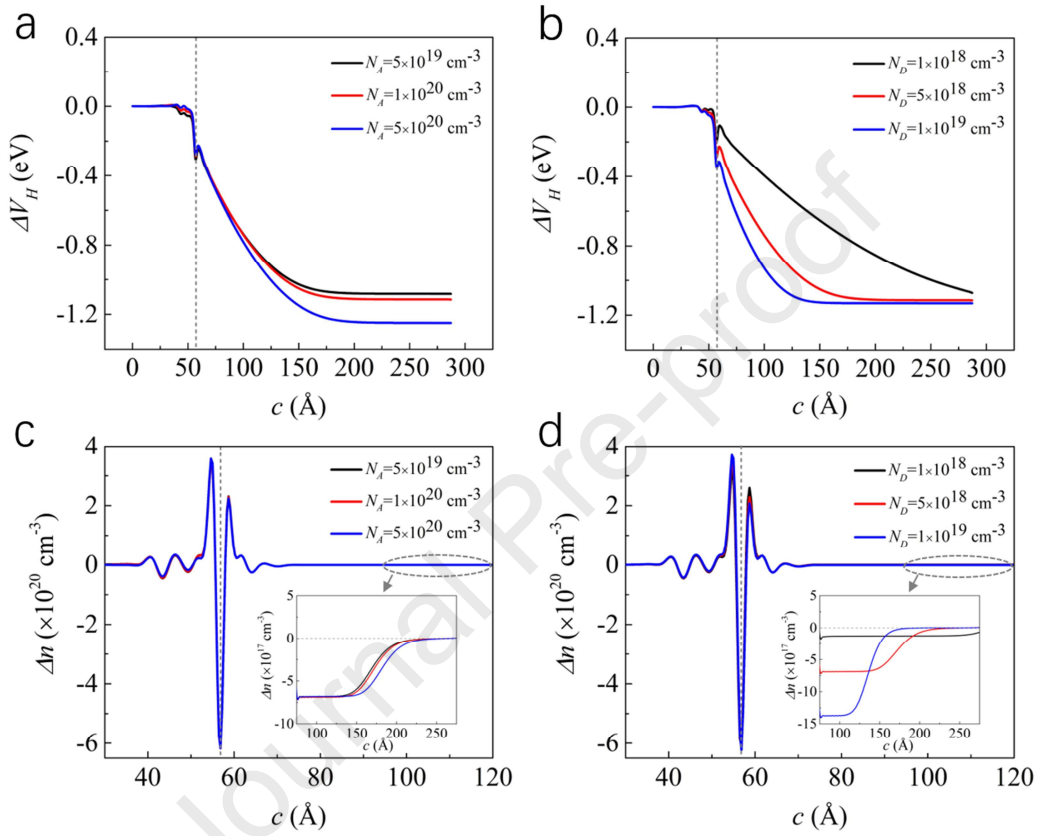

Fig. 3. The HDP and EDD for the non-ideal contacted *p-n* junctions with different doping concentrations. The vertical gray dash line marks the non-ideal contact surfaces. **a** and **b,** The HDP results for several different doping concentrations. the depletion width increases with decreasing the doping concentration. **c** and **d,** The EDD results for the corresponding doping concentrations in **a** and **b**. Hydrogen atoms (the surface passivation layer) induce an electron redistribution at the contact surfaces. The insets in **c** and **d**, The zoom-in view of the EDD.

When the *p*-type and *n*-type silicon are brought in contact, electrons (holes) transfer from *n*-(*p*-)type to *p*-(*n*-)type silicon due to their chemical potential difference. A built-in electric field is concurrently created and it then resists the diffusion so that a *p-n* junction is eventually established at thermal equilibrium. The chemical potential difference between the two silicon electrodes is fully dropped to the depletion regions whose widths reach their maximum. The space charges in the depletion regions are those positively ionized donors in the *n*-type silicon and negatively ionized acceptors in the *p*-type silicon. Once the *p*-type and *n*-type silicon are being separated with a

small gap, say 30 Å, most of the potential drops to the gap and, consequently, the depletion regions must shrink drastically. The energy band diagram and the HDP are shown in Figs. 4a and 4b, respectively. The depletion region width w_n' (Fig. 4b) is much smaller than W_n' (Fig. 2b). The influence of the gap width, d, on the HDP distribution is illustrated in Fig. 4c. With increasing d from 0 to 180 Å, the depletion region width of the *n*-type silicon decreases from about 170 Å down to 29 Å. In contrast, the EDD at the surface or surface charge maintains nearly unchanged. (Fig. 4d).

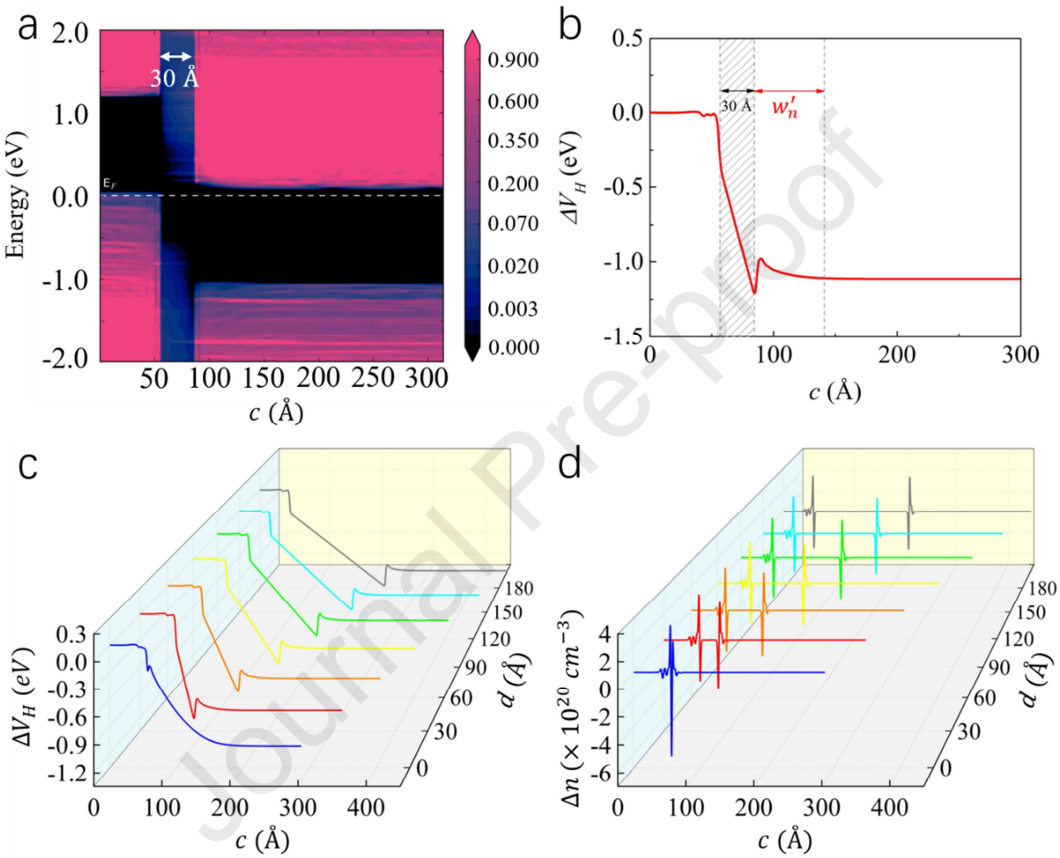

Fig. 4. The energy band diagram, HDP and EDD for the relaxed silicon electrodes with a steady separation gap. a and **b**, The energy band diagram and HDP result for the two non-ideal n-type and p-type silicon electrode with a steady separation gap of 30 Å. Most of the potential drops to the air gap and the depletion regions shrink drastically. **c** and **d,** The influence of the gap width d on the HDP and EDD, respectively. With increasing d, the depletion region width of the *n*-type silicon decreases significantly, while the EDD at the surface maintains nearly unchanged.

Under the thermal equilibrium, the space charge density, $N_c(x)$, in the *n*-type silicon can be determined by the difference between the ionized donor concentration and local electron concentration. The local electron concentration can be obtained from the Boltzmann approximation and the potential distribution. In the depletion region of the *n*-type silicon electrode, electron concentration is much lower than the donor concentration so that $N_c(x)$ equals the donor concentration of $5 \times 10^{18}\ cm^{-3}$, while

$N_c(x)$ decreases to about zero at the edge of the depletion region (Fig. 5a), yielding $W_n' = 170$ Å in the contacted stage. Thus, the total space charge is, $Q_s = eA\int_0^{W_n'} N_c(x)dx = 3.8 \times 10^{-6}\ C$ for the *p-n* junction area $A = 4\ cm^2$. Note that as W_n' is smaller than $W_n\ (= 195$ Å$)$ for the ideal *p-n* junction, Q_s is a factor of 1.7 smaller than the amount of total space charges for the ideal contact *p-n* junction ($\sim 4.4 \times 10^{-6}\ C$). This result indicates that existence of the surface charges has a negative impact on not only electron transfer (discussed above), but also the space charges stored in the depletion region. After the two electrodes are separated by a steady separation gap d from 0 to 30 Å with a step of 5 Å, the depletion width decreases from 170 to 102, 82, 69, 60, 54 and 51 Å, respectively (Figs. 5a and 5b). Obviously, the initial several separations cause much more significant shrinking in the depletion region w_n'. For $d > 30$ Å, the space charge concentration distribution shows less significant change (Fig. 5b). The amount of the charges that can be pumped to the circuit is $\Delta Q = Q_s - Ae\int_0^{w_n'} N_c(x)dx = Ae\int_{w_n'}^{W_n'} N_c(x)dx$. ΔQ as a function of d in Fig. 5c shows that the main charge 'pumping' occurs for $d < 30$ Å. The efficiency of the space charge 'pumping', $\Delta Q/Q_s \times 100\%$, is as large as 68% for $d = 30$ Å (Fig. 5d). Moreover, the amount of charge 'pumping' for $d = 30$ Å is about $2.6 \times 10^{-6}\ C$, which is more than 2 orders of magnitude larger than the charge pumping for d from 150 to 180 Å ($2.0 \times 10^{-8}\ C$). It is worth noting that $\Delta Q/Q_s \times 100\%$ increases with d and it then tends to be saturated for $d \geq 60$ Å. This is caused by the surface charges or a surface potential barrier, which hinders the space charge being fully pumped out. The tunneling probability is analyzed using the Wentzel-Kramers-Brillouin approximation [35] and it is only ~ 0.08 for a gap of 5 Å, implying that the tunneling effect does not play an important role here and it can be ignored for $d > 5$ Å.

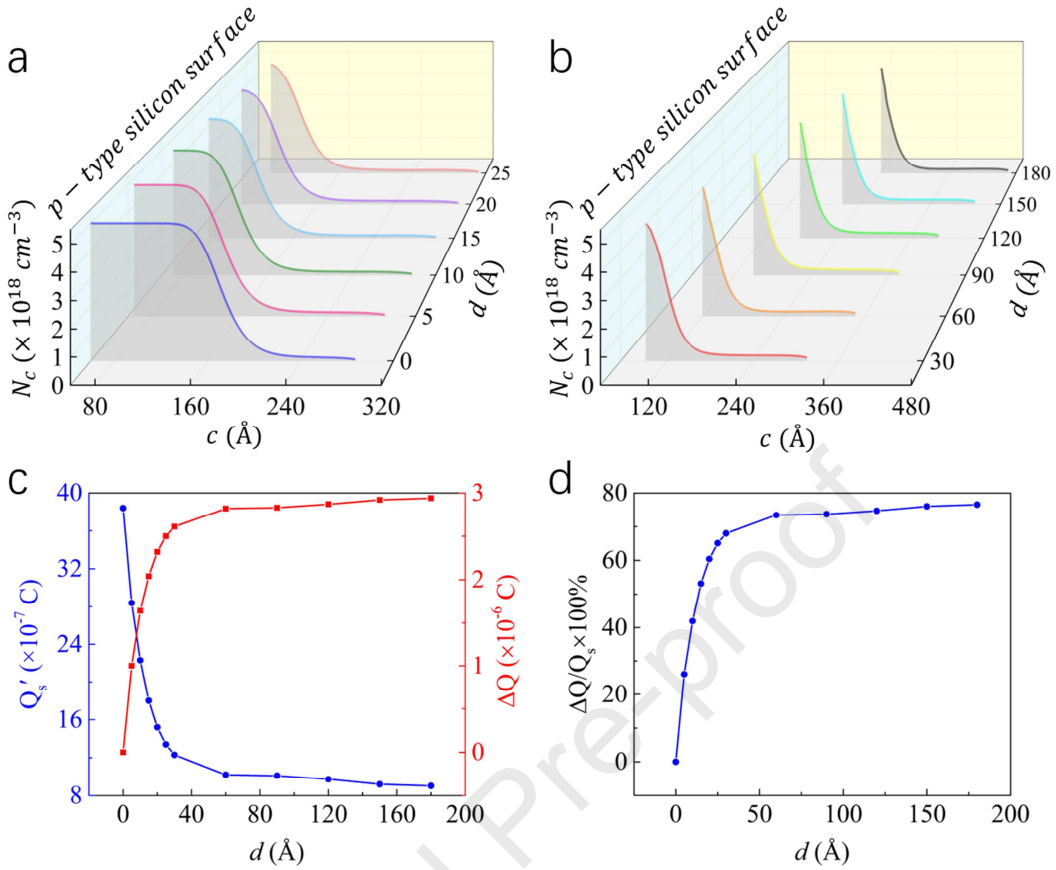

Fig. 5. Influences of a steady separation gap width from 0 to 180 Å on the space charge distribution in the non-ideal *n*-type silicon electrode and the charge 'pumping' property. a and **b**, The space charge distributions for different separation gap widths. The initial several separations cause much more significant shrinking in the depletion region. **c** and **d,** The amount of the charge remained in the depletion region Q_s', charge pumped out to the circuit ΔQ and the charge pumping efficiency $\Delta Q/Q_s$ as a function of d.

In our prior experiments [1], the collected charge in the circuit was found to be 3 ~ 4 orders of magnitude smaller than the space charge stored in a corresponding ideal *p-n* junction. In view of the first-principles study presented here, the huge difference could originate from two main factors: (1) A high density of surface charges exist at the silicon electrode surfaces due to the surface relaxation and hydrogenation treatment. The surface charges hinder not only electron and hole diffusion across the non-ideal contacted surfaces but also the charge pumped out of the depletion region. An appropriate surface treatment may help to control surface charge. In our prior work [1], we reported that HF treatment of silicon electrode surface could control surface charges. Although different oriented silicon surfaces have different densities of dangling bonds, which induce different densities of surface charges at the silicon electrode surfaces, the chemical potential difference between both electrodes is dependent on the doping concentrations of the two silicon electrodes, rather than the silicon orientations. Thus, the above conclusion acquired from silicon (100) surface is

still applicable for other silicon surfaces. (2) A small air gap exists between the contacted surfaces due to existence of the atomic-scale asperities. As the experiments were carried out with the electrode areas of $4\ cm^2$, actual contact could be through a number of the asperities, leaving most of contacted surfaces with a small air gap. This could largely reduce the charge pumping efficiency. Above all, the unique electric generator could have a leap in the charge pumping performance if the surface charge and small air gap are well controlled. As a feasible approach, a small air gap could be reduced by utilizing a soft semiconductor as one of the contact electrodes or liquid metal contact, etc [36, 37]. The characteristic that a small gap of $30\ Å$ could lead to 68% of the charge to be 'pumped' to the circuit can be a remarkable advantage over other electric generators for detection and/or energy harvesting of ultrahigh frequency small displacement mechanical motions.

Conclusion:

We have studied the influences of the surface charge and separation gap between a *p*-type and *n*-type silicon electrode on the space charges in the depletion region using the first principles calculation with NEGF. The surface charges have a significant impact on the electric potential distribution in the depletion region, hindering electron and hole transfer across the contacted surfaces and charge pumping. With a small air gap of several nanometers, most of the charge stored in the depletion region of the contacted *p*-*n* junction can be 'pumped' out to the external circuit.

Declaration of competing interest:

The authors declare that they have no known competing financial interests or personal relationships that could have appeared to influence the work reported in this paper.

Acknowledgments:

This project is financially support by MOE AcRF Tier1 (2018-T1-005-001), MOE AcRF Tier2 (2018-T2-2-005) and A*STAR AME IRG Grant SERC A1983c0027, Singapore; European Regional Development Fund (ERDF) for the funding of the Solar Photovoltaic Academic Research Consortium (SPARC II); National Natural Science Foundation of China (11974266 and 51805395); Natural Science Foundation of Hubei Province (20181j001).

References:

[1] Q. Zhang, R. Xu, W.F. Cai, Pumping electrons from chemical potential difference, Nano Energy 51 (2018) 698-703.

[2] D.P. Arnold, Review of microscale magnetic power generation, Ieee Trans. Magn. 43 (2007) 3940-3951.

[3] J.M. Donelan, Q. Li, V. Naing, J.A. Hoffer, D.J. Weber, A.D. Kuo, Biomechanical energy harvesting: Generating electricity during walking with minimal user effort, Science 319 (2008) 807-810.

[4] Y. Wang, Q. Zhang, L. Zhao, Y. Tang, A. Shkel, E.S. Kim, Vibration energy harvester with low resonant frequency based on flexible coil and liquid spring, Appl. Phys. Lett. 109 (2016) 203901.

[5] P.V. Malaji, S.F. Ali, Magneto-mechanically coupled electromagnetic harvesters for broadband energy harvesting, Appl. Phys. Lett. 111 (2017) 083091.

[6] Y.S. Tan, Y. Dong, X.H. Wang, Review of mems electromagnetic vibration energy harvester, J. Microelectromech. S. 26 (2017) 1-16.

[7] S. Meninger, J.O. Mur-Miranda, R. Amirtharajah, A.P. Chandrakasan, J.H. Lang, Vibration-to-electric energy conversion, Ieee Trans. Vlsi. Syst. 9 (2001) 64-76.

[8] P.D. Mitcheson, P. Miao, B.H. Stark, E.M. Yeatman, A.S. Holmes, T.C. Green, Mems electrostatic micropower generator for low frequency operation, Sensor Actuat a-Phys. 115 (2004) 523-529.

[9] Z.L. Wang, J.H. Song, Piezoelectric nanogenerators based on zinc oxide nanowire arrays, Science 312 (2006) 242-246.

[10] Y. Chiu, V.F.G. Tseng, A capacitive vibration-to-electricity energy converter with integrated mechanical switches, J. Micromech. Microeng. 18 (2008) 104004.

[11] F.R. Fan, Z.Q. Tian, Z.L. Wang, Flexible triboelectric generator, Nano Energy 1 (2012) 328-334.

[12] P. Basset, D. Galayko, A.M. Paracha, F. Marty, A. Dudka, T. Bourouina, A batch-fabricated and electret-free silicon electrostatic vibration energy harvester, J. Micromech. Microeng. 19 (2009) 115025.

[13] Y.L. Zhang, T.Y. Wang, A.X. Luo, Y.S. Hu, X. Li, F. Wang, Micro electrostatic energy harvester with both broad bandwidth and high normalized power density, Appl. Energ. 212 (2018) 362-371.

[14] Z.B. Wu, M.Z. Bi, Z.Y. Cao, S.W. Wang, X.Y. Ye, Largely enhanced electrostatic generator based on a bipolar electret charged by patterned contact micro-discharge and optimized substrates, Nano Energy 71 (2020) 104602.

[15] B.Y. Lee, J.X. Zhang, C. Zueger, W.J. Chung, S.Y. Yoo, E. Wang, J. Meyer, R. Ramesh, S.W. Lee, Virus-based piezoelectric energy generation, Nat. Nanotechnol. 7 (2012) 351-356.

[16] W.Z. Wu, L. Wang, Y.L. Li, F. Zhang, L. Lin, S.M. Niu, D. Chenet, X. Zhang, Y.F. Hao, T.F. Heinz, J. Hone, Z.L. Wang, Piezoelectricity of single-atomic-layer mos2 for energy conversion and piezotronics, Nature 514 (2014) 470.

[17] R.G. Horn, D.T. Smith, Contact electrification and adhesion between dissimilar materials, Science 256 (1992) 362-364.

[18] Z.L. Wang, J. Chen, L. Lin, Progress in triboelectric nanogenerators as a new energy technology and self-powered sensors, Energ. Environ. Sci. 8 (2015) 2250-2282.

[19] Z.L. Wang, On maxwell's displacement current for energy and sensors: The origin of nanogenerators, Mater. Today 20 (2017) 74-82.

[20] M. Brandbyge, J.L. Mozos, P. Ordejon, J. Taylor, K. Stokbro, Density-functional method for nonequilibrium electron transport, Phys. Rev. B 65 (2002) 165401.

[21] S.H. Shin, Y.E. Bae, H.K. Moon, J. Kim, S.H. Choi, Y. Kim, H.J. Yoon, M.H. Lee, J. Nah, Formation of triboelectric series via atomic-level surface functionalization for triboelectric energy harvesting, ACS Nano 11 (2017) 6131-6138.

[22] J. Wu, X.L. Wang, H.Q. Li, F. Wang, W.X. Yang, Y.Q. Hu, Insights into the mechanism of metal-polymer contact electrification for triboelectric nanogenerator via first-principles investigations, Nano Energy 48 (2018) 607-616.

[23] J. Wu, X.L. Wang, H.Q. Li, F. Wang, Y.Q. Hu, First-principles investigations on the contact electrification mechanism between metal and amorphous polymers for triboelectric nanogenerators, Nano Energy 63 (2019) 103864.

[24] L.Z. Li, X.L. Wang, P.Z. Zhu, H.Q. Li, F. Wang, J. Wu, The electron transfer mechanism between

metal and amorphous polymers in humidity environment for triboelectric nanogenerator, Nano Energy 70 (2020) 104476.

[25] R. Xu, Q. Zhang, J.Y. Wang, D. Liu, J. Wang, Z.L. Wang, Direct current triboelectric cell by sliding an n-type semiconductor on a p-type semiconductor, Nano Energy 66 (2019) 104185.

[26] Z. Zhang, D.D. Jiang, J.Q. Zhao, G.X. Liu, T.Z. Bu, C. Zhang, Z.L. Wang, Tribovoltaic effect on metal-semiconductor interface for direct-current low-impedance triboelectric nanogenerators, Adv. Energy. Mater. 10 (2020) 1903713.

[27] M.L. Zheng, S.Q. Lin, L. Xu, L.P. Zhu, Z.L. Wang, Scanning probing of the tribovoltaic effect at the sliding interface of two semiconductors, Adv. Mater. 32 (2020) 2000928.

[28] S. Smidstrup, T. Markussen, P. Vancraeyveld, J. Wellendorff, J. Schneider, T. GunstL, B. Verstichel, D. Stradi, P.A. Khomyakov, U.G. Vej-Hansen, M.E. Lee, S.T. Chill, F. Rasmussen, G. Penazzi, F. Corsetti, A. Ojanpera, K. Jensen, M.L.N. Palsgaard, U. Martinez, A. Blom, M. Brandbyge, K. Stokbro, Quantumatk: An integrated platform of electronic and atomic-scale modelling tools, J. Phys-Condens. Mat. 32 (2020) 015901.

[29] M. Palsgaard, T. Markussen, T. Gunst, M. Brandbyge, K. Stokbro, Efficient first-principles calculation of phonon-assisted photocurrent in large-scale solar-cell devices, Phys. Rev. Appl. 10 (2018) 014026.

[30] S. Smidstrup, D. Stradi, J. Wellendorff, P.A. Khomyakov, U.G. Vej-Hansen, M.E. Lee, T. Ghosh, E. Jonsson, H. Jonsson, K. Stokbro, First-principles green's-function method for surface calculations: A pseudopotential localized basis set approach, Phys. Rev. B 96 (2017) 195309.

[31] J.P. Perdew, K. Burke, M. Ernzerhof, Generalized gradient approximation made simple, Phys. Rev. Lett. 77 (1996) 3865-3868.

[32] A. Ramstad, G. Brocks, P.J. Kelly, Theoretical-study of the si(100) surface reconstruction, Phys. Rev. B 51 (1995) 14504-14523.

[33] A.D. Becke, M.R. Roussel, Exchange holes in inhomogeneous systems - a coordinate-space model, Phys. Rev. A 39 (1989) 3761-3767.

[34] F. Tran, P. Blaha, Accurate band gaps of semiconductors and insulators with a semilocal exchange-correlation potential, Phys. Rev. Lett. 102 (2009) 226401.

[35] J.G. Simmons, Generalized formula for the electric tunnel effect between similar electrodes separated by a thin insulating film, J. Appl. Phys. 34 (1963) 1793.

[36] W. Tang, T. Jiang, F.R. Fan, A.F. Yu, C. Zhang, X. Cao, Z.L. Wang, Liquid-metal electrode for high-performance triboelectric nanogenerator at an instantaneous energy conversion efficiency of 70.6%, Adv. Funct. Mater. 25 (2015) 3718-3725.

[37] J.Q. Xiong, P. Cui, X.L. Chen, J.X. Wang, K. Parida, M.F. Lin, P.S. Lee, Skin-touch-actuated textile-based triboelectric nanogenerator with black phosphorus for durable biomechanical energy harvesting, Nat. Commun. 9 (2018) 4280.

Author Biosketch:

Dr. Shuo Deng received his Ph.D. degree from Wuhan University of Technology in 2019. In 2017, Shuo joined College of Engineering, Swansea University, UK, as a visiting student for two years. His current research focuses on theoretical and experimental investigation of electric generators and sensors based on semiconductor junctions.

Ran Xu is currently a Ph.D. candidate in School of Electrical and Electronic Engineering, Nanyang Technological University (NTU), Singapore. She received her B.S degree from School of Electrical and Electronic Engineering, Nanyang Technological University in 2015. Her research interests are in the area of electric generators based on dynamic semiconductor junctions.

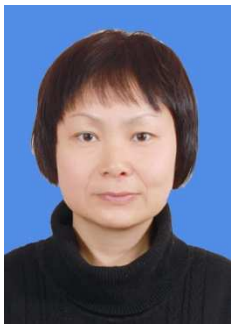

Prof. Min Li received her Ph.D. degree from Department of Electronic Engineering of Tsinghua University in 1999. Now, she is the director of Department of Physics, Wuhan University of Technology. In 2010, Min joined University of Strathclyde, UK, as a visiting scholar. Min's research interests are widespread over strain, temperature, gas, biomedical sensors and their applications.

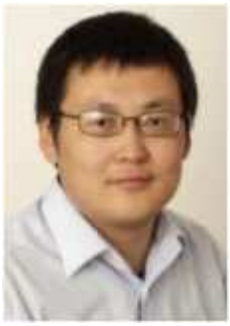

Lijie Li is a professor at Swansea University, UK. His research interests are design, modeling, fabrication, and characterization of MEMS, NEMS, sensors and actuators. He is Fellow of IET, and senior member of IEEE.

Prof. Zhong Lin (ZL) Wang is the Hightower Chair in Materials Science and Engineering and Regents' Professor at Georgia Tech, the chief scientist and director of the Beijing Institute of Nanoenergy and Nanosystems, Chinese Academy of Sciences. His discovery and breakthroughs in developing nanogenerators and self-powered nanosystems establish the principle and technological road map for harvesting mechanical energy from environmental and biological systems for powering personal electronics and future sensor networks. He coined and pioneered the field of piezotronics and piezophototronics.

Qing Zhang is a full professor in School of Electrical and Electronic Engineering, Nanyang Technological University (NTU), Singapore. His research interests cover nanomaterials and nano/micro- electronic devices, carbon/silicon based thin films, etc. His attention focuses on carbon nanotube and nanostructure-based devices and fundamentals, etc. He and his group members have studied functionalized carbon nanotubes for several types of sensors, logic circuits and Li-ion batteries, etc. Currently, he is interested in electric generators based on semiconductor junctions.

Highlights:

(1) A large density of states are formed during silicon surface relaxation and they are further changed during hydrogenated process.

(2) The surface charges result in a surface potential barrier, which has a negative impact on electron and hole transfer between the contacted silicon surfaces.

(3) The total charges in the depletion regions depend very sensitively on the air gap between the two silicon electrodes.

(4) Intermittently contacted *p*-*n* junction could function as an efficient electric generator or mechanical sensor if the surface states and gap width are well controlled.

Declaration of interests

☒ The authors declare that they have no known competing financial interests or personal relationships that could have appeared to influence the work reported in this paper.

☐The authors declare the following financial interests/personal relationships which may be considered as potential competing interests: